Intensity-Based Axial Localization at the Quantum Limit

J. Řeháček,[1] M. Paúr,[1] B. Stoklasa,[1] D. Koutný,[1] Z. Hradil,[1] and L. L. Sánchez-Soto[2,3]
[1]Department of Optics, Palacký University, 17. listopadu 12, 771 46 Olomouc, Czech Republic
[2]Departamento de Óptica, Facultad de Física, Universidad Complutense, 28040 Madrid, Spain
[3]Max-Planck-Institut für die Physik des Lichts, Staudtstraße 2, 91058 Erlangen, Germany

(Received 20 June 2019; published 7 November 2019)

We derive fundamental precision bounds for single-point axial localization. For Gaussian beams, this ultimate limit can be achieved with a single intensity scan, provided the camera is placed at one of two optimal transverse detection planes. Hence, for axial localization there is no need of more complicated detection schemes. The theory is verified with an experimental demonstration of axial resolution 3 orders of magnitude below the classical depth of focus.

DOI: 10.1103/PhysRevLett.123.193601

Introduction.—The maximum spatial resolution attainable in classical microscopy is usually established in terms of the Abbe-Rayleigh criterion [1,2]. However, it is well known that this criterion is based on heuristic notions and is an inadequate performance measure for current quantitative imaging [3,4].

Indeed, several modern techniques, gathered under the broad denomination of superresolution microscopy [5–9], are capable of achieving a striking increase in resolution by more than one order of magnitude in comparison with the length scale set by the Abbe-Rayleigh criterion. An important class of these techniques (which includes, among others, stimulated-emission-depletion microscopy [10], photoactivated-localization microscopy [11], point spread function (PSF) engineering [12–16], and multiplane detection [17–19]) relies on a very accurate localization of point sources.

For three-dimensional imaging, extracting the emitter axial position is an enduring challenge that has been extensively investigated [20]. Yet, finding the optimal depth precision attainable by any such microscope engineering approach has been only recently tackled [21,22]. The basic idea is to use the quantum Fisher information (QFI) and the associated Cramér-Rao bound (QCRB) to get a measurement-independent limit [23], much in the same vein as Tsang and co-workers did to quantify transverse two-point resolution [24–27] (see also Ref. [28]).

In this Letter, we address this fundamental question from a different perspective. By identifying the unitary transformation that embodies the action of the system and its corresponding generator, we get in a very transparent way the ensuing QCRB. More important, we do find the optimal measurement reaching such a limit.

We focus here on direct imaging, for this is the simplest method available in the laboratory. Of course, one could rightly argue that in this way all the phase information is wasted. Surprisingly, we demonstrate that direct detection can saturate the quantum limits with a single intensity scan, as long as the camera is placed in one optimal transverse detection plane. This might be of utmost importance for any application demanding extreme stringent localization, as it only requires very simple and feasible equipment.

Theoretical model.—To simplify the details as much as possible, we take the waist of a focused beam as our object. The task is to estimate the distance from this object to a detection plane. In the following, we shall use the Dirac notation to represent the field, as it allows us to extend the theory to any type of light source.

If the beam in the object plane is represented by the pure state $|\Psi(0)\rangle$, the axial displacement can be described by a unitary operation $|\Psi(z)\rangle = e^{iGz}|\Psi(0)\rangle$, the Hermitian operator G being the corresponding generator. To identify the action of G in a more precise way, it is convenient to use the transverse-position representation $\Psi(x, y; z) = \langle x, y|\Psi(z)\rangle$. Given our unitary parametrization, it holds

$$\partial_z \Psi(x, y; z) = iG\Psi(x, y; z), \tag{1}$$

which is consistent with the paraxial wave equation $2ik\partial_z \Psi(x, y; z) = \nabla_T^2 \Psi(x, y; z)$ if $G \mapsto (1/2k)\nabla_T^2$, where k is the wave number and $\nabla_T^2 = \partial_{xx} + \partial_{yy}$ is the transverse Laplacian.

For a more tractable analysis and experiment, here we assume a normalized Gaussian beam

$$\Psi(r; z) = \frac{2}{w(z)} e^{-\{r^2/[w^2(z)]\}} \exp\left[-i\left(kz + \frac{kr^2}{2R(z)} - \phi(z)\right)\right], \tag{2}$$

although the results are largely independent of this choice. Notice that, given the cylindrical symmetry, the beam depends exclusively on the radial coordinate r. The field distribution in Eq. (2) is determined by the beam waist w_0 and

the Rayleigh range z_R through $w^2(z) = w_0^2[1 + (z/z_R)^2]$, $R(z) = z[1 + (z_R/z)^2]$, $\phi(z) = \arctan(z/z_R)$, and $z_R = \pi w_0^2/\lambda$.

The detection plane is placed at z and therein we perform a measurement that we do not need to specify beforehand. To quantify the information about z available in the measured signal we use the QFI, which, for pure states, as it is our case, is given by $\mathcal{Q}(z) = 4\ \mathrm{Var}(G)$, where Var is the variance computed in the initial state. Given the explicit form of G in the transverse representation, a direct calculation shows that for the Gaussian beam one has

$$\mathcal{Q}(z) = \frac{1}{z_R^2}, \tag{3}$$

which turns out to be constant. The QCRB [29,30] ensures then that the variance of any unbiased estimator $\hat{z}$ of the displacement z is bounded by the reciprocal of the QFI; viz, $\mathrm{Var}(\hat{z}) \geq z_R^2$. As a consequence, the lower bound on axial-measurement errors (per single detection) is precisely the Rayleigh range. This agrees with the result recently found in Ref. [31], which discusses the ultimate limits for two-point axial resolution.

Direct detection.—In general, the QFI is distributed between the phase and intensity variations of the measured beam. One thus would naively conclude that intensity detection, discarding all phase information, cannot saturate the quantum limit (3). We will show that, contrary to this belief, this is not the case when the detector is appropriately placed.

We model the light detection as a random process and, consequently, we interpret the normalized beam intensity $p(r|z) = |\Psi(r; z)|^2$ as the probability density of a single detection event at r conditional on the value of z. We assume that detection is limited by shot noise, which obeys a Poisson distribution [32]. This simplified approach ignores nonclassical effects, as bunching or entanglement, but is nonetheless relevant to practical microscopy. In addition, we ignore finite spatial extent and nonzero pixel size. Under these hypothesis, the classical Fisher information about z per single detection is

$$\mathcal{F}(z) = 2\pi \int_0^\infty r \frac{[\partial_z p(r|z)]^2}{p(r|z)} dr, \tag{4}$$

and the associated Cramer-Rao bound quantifies the axial localization error for direct detection. For a Gaussian beam, $p(r|z) = [\pi w^2(z)/2]^{-1} \exp[-2r^2/w^2(z)]$, so that

$$\mathcal{F}(z) = \left[\frac{\partial_z w^2(z)}{w^2(z)}\right]^2 = \frac{4}{R^2(z)} = \frac{4}{z^2[1 + (z_R/z)^2]^2}. \tag{5}$$

Optimal detector positions are at the planes of maximal wave front curvature: $z_{\mathrm{opt}} = \pm z_R$, whereby the quantum limit is saturated; i.e., $\mathcal{F}_{\mathrm{opt}} = 1/z_R^2$. In these planes, all the information about the axial waist location is conveyed by the intensity and can be extracted with conventional imaging, thus avoiding more complicated and less robust techniques.

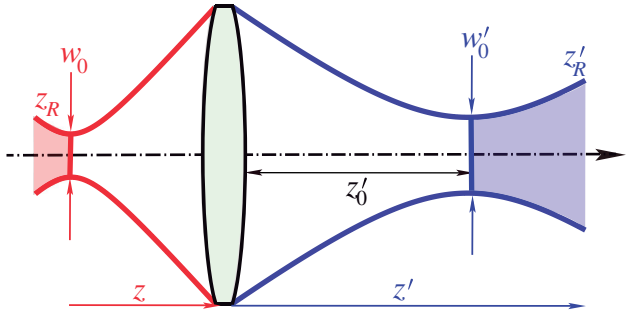

FIG. 1. Scheme of the axial localization experiment with a relay optical system.

Potential applications of this effect benefit from using a relay optical system for reimaging the object and obtaining a more convenient detector position. Figure 1 sketches the simplest case of a thin lens placed a distance z from the waist. Primed symbols will distinguish henceforth parameters in the image space.

Since an ideal imaging system applies a unitary transformation, the QFI does not change from the object space to the image space: $\mathcal{Q}' = \mathcal{Q}$. Recalling the standard relations [33]

$$w_0'^2 = m^2 w_0^2, \qquad z_R' = m^2 z_R, \qquad z_0' = m^2(z - f) + f, \tag{6}$$

between the original and new beam parameters, where $m = f/[(z - f)^2 + z_R^2]^{1/2}$ is the magnification, we find the beam width at the detector position z' to be

$$w'^2(z') = w_0'^2 \left[1 + \left(\frac{z' - z_0'}{z_R'}\right)^2\right]. \tag{7}$$

Much in the same way as in Eq. (5), we have now

$$\mathcal{F}'(z) = \left[\frac{\partial_z w'^2(z')}{w'^2(z')}\right]^2 = \frac{4(f - z')^2[zz' - f(z + z')]^2}{\{(z^2 + z_R^2)z'^2 - 2fz'(z^2 + z_R^2 + zz') + f^2[(z + z')^2 + z_R^2]\}^2}. \tag{8}$$

The typical behavior of $\mathcal{F}'$ around the beam waist is shown in Fig. 2. We observe the presence of well-resolved maxima $\mathcal{F}'_{\mathrm{opt}} = \mathcal{Q}$ and minima $\mathcal{F}'_{\mathrm{min}} = 0$. While the beam in the image space is symmetric about the waist, the response of the beam width to small changes of the true distance z is different inside and outside the waist, which makes the Fisher information (FI) asymmetrical with respect to the image waist. These extremal points are located at

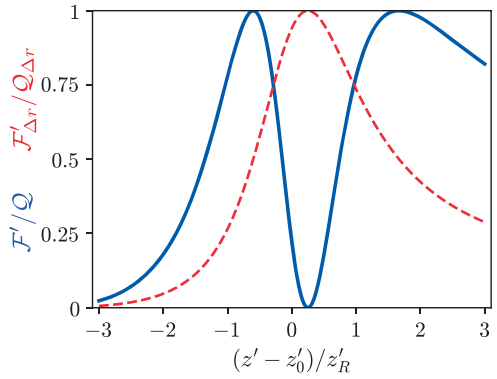

FIG. 2. Fisher information at the image space about axial (blue solid line) and transversal (red broken line) positions of the object waist in units of their respective QFI for different placements of the detector. We use $z = 5$, $f = 1$, $z_R = 1$, $w_0 = 1$ and the detector positions are relative to the beam waist in units of z'_R.

$$z'_{\text{opt}} = \begin{cases} z'_0 + \alpha z'_R, \\ z'_0 - \frac{1}{\alpha} z'_R, \end{cases} \tag{9}$$

where $\alpha = (f - z - z_R)/(f - z + z_R)$. In the geometrical limit $f - z \gg z_R$, we have $\alpha \simeq 1$ and $z'_{\text{opt}} \approx z'_0 \pm z'_R$, so the asymmetry disappears.

Observe that the information about axial displacements is zero in the plane of the geometrical image $z'_g = fz/(z - f)$, as the FI tends to zero therein. This is to be compared with the information about transversal beam localization. In this case, a small lateral shift Δr of a Gaussian object of width w_0 leads to a corresponding lateral shift of $\Delta r' = [(f - z')/f]\Delta r$ of the detected Gaussian profile of width $w'(z')$ in the plane z'. A direct calculation reveals that the resulting FI $\mathcal{F}'_r$ about Δr is maximized by placing the detector in the plane of the geometrical image z'_g, where the quantum limit is attained $\mathcal{F}'_{r,\text{opt}} = 1/w_0^2$, as can be checked in Fig. 2. In this sense, optimal axial localization (requiring considerable image blur) and transverse localization (benefiting from sharpness) complement each other. PSF engineering reaches a balance to resolve this issue and provides a good three-dimensional resolution. However, these methods always broaden the PSF, even more than our defocusing in z_R.

Experiment.—To check the previous theory we have used a classical microscopy setup, as schematized in Fig. 3. It consists of an objective corrected for infinity and a tube lens, all together providing a 20× magnification of the output face of a single mode fiber representing a Gaussian source. The fiber is coupled with a 632.8 nm He-Ne laser. As the Rayleigh range z_R at the fiber output is 18.9 μm, the camera with 5.5 μm pixel size is moved 7.6 mm out of the system nominal image plane to become aligned with one of the optimal detection positions given in Eq. (9). Controlled changes of the axial distance z were implemented by moving the fiber axially using a piezo stage with a resolution of 1 nm.

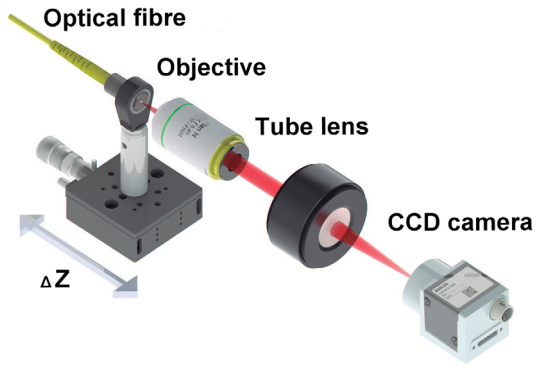

FIG. 3. Experimental setup used to measure the axial displacement z. See text for a detailed description.

Note that the integrand in Eq. (4); viz, $F(r; z) = r[\partial_z p(r|z)]^2/p(r|z)$ can be seen as a radial density of Fisher information. Using the normalized beam intensity profile in the image space, this magnitude is plot in Fig. 4 at the optimal detection plane z'_{opt}, which hints at constructing a robust estimator of axial displacement from the registered intensity scans. The information drops to zero at $r_b = w'_{\text{opt}}/\sqrt{2}$ and the bulk of information ($2/e \simeq 74\%$) resides outside this boundary in the wings of the Gaussian intensity distribution. We will call $I_{\text{det}}(z)$ the intensity outside r_b for the object distance z. Then for small displacements δ_z from the nominal position z we have

$$I_{\text{det}}(z + \delta_z) = I_{\text{det}}(z)(1 - \delta_z/z_R). \tag{10}$$

This linear relation is readily inverted to yield an estimate $\hat{\delta}_z$ of δ_z from I_{det}. Of course, we might be tempted to use the maximum likelihood estimator based on the full profile. However, this estimator turns to be a bit noisy due to systematic errors [34]. On the contrary, our estimator $\hat{\delta}_z$ is simple and robust. Nevertheless, we stress that we are

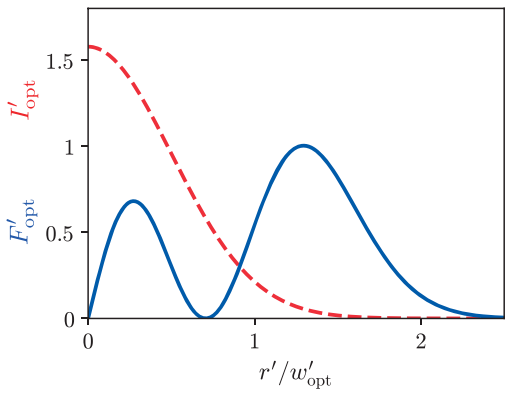

FIG. 4. Normalized radial density of Fisher information (solid blue line) and normalized beam intensity profile (dashed red line) in the optimal detection plane, where the beam has a width w'_{opt}. The system parameters are the same as in Fig. 2.

interested in a proof-of-concept experiment, so small deviations from the theoretical best performance are not an issue.

We also notice that we are assuming that the nominal axial distance is known. When this is not the case, Fig. 2 clearly indicates the loss of precision in the z estimate associated with a nonoptimal detector placement. Quite often, this is not a serious issue, as one can perform a previous calibration (as we did in the experiment), and then measure in a very precise manner around the nominal value. If this is still not applicable, one can adopt an adaptive approach, where a small part of the total resources (photons) is allocated on a nonoptimally placed detection and the detector position is refined according to the first estimate of z. This process can be repeated and the optimal detection plane hunted down in subsequent iterations.

Our experimental results are summarized in Fig. 5. Measurement errors are consistent across the full range of axial displacements $\delta_z \in [10\ \text{nm}, 1650\ \text{nm}]$ averaging 24.8 nm. This is about 800 times below the depth of focus z_R and not much above the quantum limit of 14.9 nm corresponding to the total number of 1.6×10^6 detections registered for each δ_z setting.

Thus far we have focused on axial measurements with Gaussian beams. What about *uncooperative* point sources? In this case, the source generates a spherical (parabolic) wave front, which after transiting a distance z enters an imaging system that truncates the unbounded wave with a

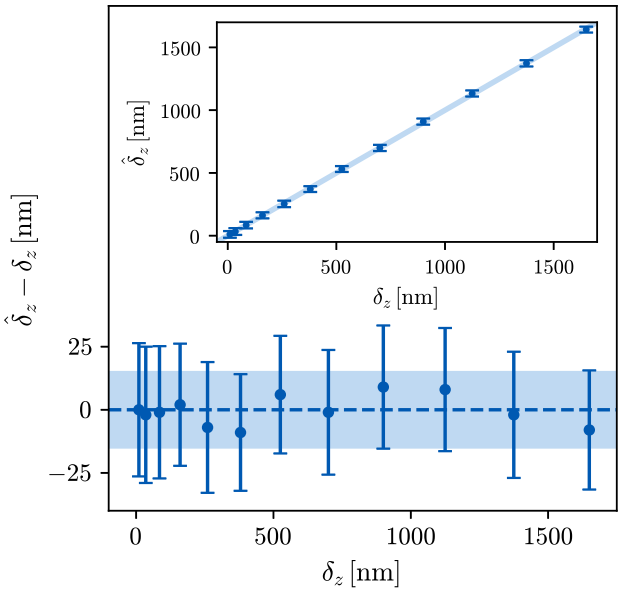

FIG. 5. Experimental estimation of axial displacements δ_z from the nominal object plane with respect to which the camera is optimally placed (9). The inset shows the statistics of the estimator $\hat{\delta}_z$ as defined in Eq. (10). In the main plot the true distance was subtracted from the estimates to get a more convenient scale on the vertical axis. The blue strips depict the quantum bound for the 2×10^6 detections and $z_R = 18.9\ \mu$m.

pupil function. Keeping things simple and considering a Gaussian pupil transmissivity of width w_l the wave transmitted by the pupil depends on z through

$$U(x, y; z) = \sqrt{\frac{2}{\pi w_l^2}} \exp\left[-\frac{r^2}{w_l^2} + i\frac{kr^2}{2}\left(\frac{1}{z} - \frac{1}{f}\right)\right]. \tag{11}$$

The state in the aperture is not just axial propagation from the point source, as the pupil acts like a filter and one needs to renormalize the state. The process is now not unitary and the QFI cannot be calculated in terms of a generator G. Instead, one has

$$\frac{1}{4}\mathcal{Q}(z) = \langle \partial_z \Psi(z) | \partial_z \Psi(z) \rangle - \langle \partial_z \Psi(z) | \Psi(z) \rangle \langle \Psi(z) | \partial_z \Psi(z) \rangle. \tag{12}$$

In contrast with a Gaussian source, the result now reads

$$\mathcal{Q}(z) = \frac{k^2 w_l^4}{4z^4}, \tag{13}$$

which strongly depends on the true distance z.

Indeed, a parabolic wave transmitted through a Gaussian apodized lens results in a Gaussian beam, which, alternatively, could have originated from a Gaussian beam and an unapodized lens. Matching the beam width at lens distance z from the Gaussian object (in the latter scenario) to the width of the lens apodization (in the former scenario) $w_l^2 = w(z)^2 \simeq w_0^2 z^2 / z_R^2 = 2z^2/(kz_R)$ means the effective Rayleigh distance of the Gaussian object simulating the point source should obey $1/z_R^2 \simeq k^2 w_l^4/(4z^4)$. Accidentally, this heuristic derivation gives the exact QFI above. Given the correspondence between the two scenarios, it is not surprising that, as for Gaussian sources, the QFI of a point source can be saturated with a single intensity scan optimally placed with respect to the nominal image plane. This is confirmed by free-space propagating (11), maximizing the classical FI associated with an intensity scan over z' and comparing the optimum to (13).

Going back to the quantum limit, it is intriguing to note that $n = 2 \times 10^6$ detections like in our experiment registered with a one meter aperture $w_l = 1$ m in visible light $k = 10^7\ \text{m}^{-1}$ would theoretically provide axial localization of a point source in a low Earth orbit $z = 200$ km with about 5 m accuracy.

In conclusion, we have theoretically and experimentally demonstrated the axial superresolution based on direct detection. The quantum limits for Gaussian beams or apertures can be saturated with a single intensity scan provided the camera is placed in one of two optimal transversal detection planes. Hence, for axial localization problem there is no advantage in adopting more complicated detection schemes. Our method makes three-dimensional superresolution imaging promising and can be

potentially useful for enhancing the resolution of optical microscopes.

We thank Robert W. Boyd for helpful discussions. We acknowledge financial support from the Czech Science Foundation (Grant No. 18-04291S), the Technology Agency of the Czech Republic (Grant No. TE01020229), the Palacký University (Grant No. IGA_PrF_2019_007), and the Spanish MINECO (Grants No. FIS2015-67963-P and No. PGC2018-099183-B-I00).

[1] L. Rayleigh, Investigations in optics, with special reference to the spectroscope, Philos. Mag. **8**, 261 (1879); Philos. Mag. **8**, 403 (1879), Philos. Mag. **8**, 477 (1879).
[2] E. Abbe, Ueber einen neuen Beleuchtungsapparat am Mikroskop, Arch. Mikrosk. Anat. **9**, 469 (1873).
[3] S. Ram, E. S. Ward, and R. J. Ober, Beyond Rayleigh's criterion: A resolution measure with application to single-molecule microscopy, Proc. Natl. Acad. Sci. U.S.A. **103**, 4457 (2006).
[4] S. Pirandola, B. R. Bardhan, T. Gehring, C. Weedbrook, and S. Lloyd, Advances in photonic quantum sensing, Nat. Photonics **12**, 724 (2018)
[5] S. W. Hell, Far-field optical nanoscopy, Science **316**, 1153 (2007).
[6] B. Huang, M. Bates, and X. Zhuang, Super-resolution fluorescence microscopy, Annu. Rev. Biochem. **78**, 993 (2009).
[7] G. Huszka and M. A. M. Gijs, Super-resolution optical imaging: A comparison, Microelectron. Eng. **2**, 7 (2019).
[8] L. Schermelleh, R. Heintzmann, and H. Leonhardt, A guide to super-resolution fluorescence microscopy, J. Cell Biol. **190**, 165 (2010).
[9] B. O. Leung and K. C. Chou, Review of super-resolution fluorescence microscopy for biology, Appl. Spectrosc. **65**, 967 (2011).
[10] S. W. Hell and J. Wichmann, Breaking the diffraction resolution limit by stimulated emission: Stimulated-emission-depletion fluorescence microscopy, Opt. Lett. **19**, 780 (1994).
[11] E. Betzig, G. H. Patterson, R. Sougrat, O. W. Lindwasser, S. Olenych, J. S. Bonifacino, M. W. Davidson, J. Lippincott-Schwartz, and H. F. Hess, Imaging intracellular fluorescent proteins at nanometer resolution, Science **313**, 1642 (2006).
[12] B. Huang, W. Wang, M. Bates, and X. Zhuang, Three-dimensional super-resolution imaging by stochastic optical reconstruction microscopy, Science **319**, 810 (2008).
[13] S. R. P. Pavani, M. A. Thompson, J. S. Biteen, S. J. Lord, N. Liu, R. J. Twieg, R. Piestun, and W. E. Moerner, Three-dimensional, single-molecule fluorescence imaging beyond the diffraction limit by using a double-helix point spread function, Proc. Natl. Acad. Sci. U.S.A. **106**, 2995 (2009).
[14] S. Jia, J. C. Vaughan, and X. Zhuang, Isotropic three-dimensional super-resolution imaging with a self-bending point spread function, Nat. Photonics **8**, 302 (2014).
[15] F. Tamburini, G. Anzolin, G. Umbriaco, A. Bianchini, and C. Barbieri, Overcoming the Rayleigh Criterion Limit with Optical Vortices, Phys. Rev. Lett. **97**, 163903 (2006).
[16] M. Paúr, B. Stoklasa, J. Grover, A. Krzic, L. L. Sánchez-Soto, Z. Hradil, and J. Řeháček, Tempering Rayleigh's curse with PSF shaping, Optica **5**, 1177 (2018).
[17] P. A. Dalgarno, H. I. C. Dalgarno, A. Putoud, R. Lambert, L. Paterson, D. C. Logan, D. P. Towers, R. J. Warburton, and A. H. Greenaway, Multiplane imaging and three dimensional nanoscale particle tracking in biological microscopy, Opt. Express **18**, 877 (2010).
[18] M. F. Juette, T. J. Gould, M. D. Lessard, M. J. Mlodzianoski, B. S. Nagpure, B. T. Bennett, S. T. Hess, and J. Bewersdorf, Three-dimensional sub–100 nm resolution fluorescence microscopy of thick samples, Nat. Methods **5**, 527 (2008).
[19] S. Abrahamsson, J. Chen, B. Hajj, S. Stallinga, A. Y. Katsov, J. Wisniewski, G. Mizuguchi, P. Soule, F. Mueller, C. D. Darzacq, X. Darzacq, C. Wu, C. I. Bargmann, D. A. Agard, M. Dahan, and M. G. L. Gustafsson, Fast multicolor 3D imaging using aberration-corrected multifocus microscopy, Nat. Methods **10**, 60 (2013).
[20] A. von Diezmann, Y. Shechtman, and W. E. Moerner, Three-dimensional localization of single molecules for super-resolution imaging and single-particle tracking, Chem. Rev. **117**, 7244 (2017).
[21] M. Tsang, Quantum limits to optical point-source localization, Optica **2**, 646 (2015).
[22] M. P. Backlund, Y. Shechtman, and R. L. Walsworth, Fundamental Precision Bounds for Three-Dimensional Optical Localization Microscopy with Poisson Statistics, Phys. Rev. Lett. **121**, 023904 (2018).
[23] D. Petz and C. Ghinea, Introduction to Quantum Fisher Information, in *Quantum Probability and Related Topics* (World Scientific, Singapore, 2011), Vol. 27, pp. 261–281.
[24] M. Tsang, R. Nair, and X.-M. Lu, Quantum Theory of Superresolution for Two Incoherent Optical Point Sources, Phys. Rev. X **6**, 031033 (2016).
[25] R. Nair and M. Tsang, Far-Field Superresolution of thermal Electromagnetic Sources at the Quantum Limit, Phys. Rev. Lett. **117**, 190801 (2016).
[26] S. Z. Ang, R. Nair, and M. Tsang, Quantum limit for two-dimensional resolution of two incoherent optical point sources, Phys. Rev. A **95**, 063847 (2017).
[27] M. Tsang, Subdiffraction incoherent optical imaging via spatial-mode demultiplexing, New J. Phys. **19**, 023054 (2017).
[28] C. Lupo and S. Pirandola, Ultimate Precision Bound of Quantum and Subwavelength Imaging, Phys. Rev. Lett. **117**, 190802 (2016).
[29] C. W. Helstrom, *Quantum Detection and Estimation Theory* (Academic, New York, 1976).
[30] A. S. Holevo, *Probabilistic and Statistical Aspects of Quantum Theory*, 2nd ed. (North Holland, Amsterdam, 2003).
[31] Y. Zhou, J. Yang, J. D. Hassett, S. M. H. Rafsanjani, M. Mirhosseini, A. N. Vamivakas, A. N. Jordan, Z. Shi, and R. W. Boyd, Quantum-limited estimation of the axial

separation of two incoherent point sources, Optica **6**, 534 (2019).

[32] D. R. Fuhrmann, C. Preza, J. A. O'Sullivan, D. L. Snyder, and W. H. Smith, Spectrum estimation from quantum-limited interferograms, IEEE Trans. Signal Process. **52**, 950 (2004).

[33] A. E. Siegman, *Lasers* (Oxford University Press, Oxford, 1986).

[34] C. S Smith, N. Joseph, B. Rieger, and K. A. Lidke, Fast, single-molecule localization that achieves theoretically minimum uncertainty, Nat. Methods **7**, 373 (2010).